Ceramics International 46 (2020) 1216–1219

Contents lists available at ScienceDirect

Ceramics International

journal homepage: www.elsevier.com/locate/ceramint

Short communication

Liquid–solid–solution synthesis of ultrafine $Gd_2Zr_2O_7$ nanoparticles with yield enhancement

Yao Yang[a,b], Zhangyi Huang[a,b], Chen Shi[a,c], Junjing Duan[a,c], Gang Cheng[a,b,c], Haomin Wang[d], Di Wu[e,f,g,h], Jianqi Qi[a,b,c,*], Tiecheng Lu[a,b,c,**]

[a] College of Physics, Sichuan University, Chengdu, 610064, China
[b] Key Laboratory of Radiation Physics and Technology of Ministry of Education, Sichuan University, Chengdu, 610064, China
[c] Key Laboratory of High Energy Density Physics of Ministry of Education, Sichuan University, Chengdu, 610064, China
[d] Institute for Advanced Study, Chengdu University, Chengdu, 610106, China
[e] Alexandra Navrotsky Institute for Experimental Thermodynamics, Washington State University, Pullman, WA, 99164, United States
[f] Voiland School of Chemical Engineering and Bioengineering, Washington State University, Pullman, WA, 99164, United States
[g] Department of Chemistry, Washington State University, Pullman, WA, 99164, United States
[h] Materials Science and Engineering, Washington State University, Pullman, WA, 99164, United States

ARTICLE INFO

Keywords:
$Gd_2Zr_2O_7$
Nanoparticle
Modified LSS method

ABSTRACT

A modified **liquid–solid–solution (LSS)** phase transfer method has been applied to synthesize $Gd_2Zr_2O_7$ binary oxide nanoparticles. X-ray diffraction (XRD), Fourier transform infrared spectroscopy (FTIR), transmission electron microscopy (TEM), thermogravimetric analysis (TG) and differential scanning calorimetry (DSC) were employed to reveal the structural, morphological and energetic evolutions of both precursors and $Gd_2Zr_2O_7$ nanoparticle products. The $Gd_2Zr_2O_7$ nanoparticles synthesized using this method exhibit an average crystallite size of 1.7 nm, which have great potential to be applied in thermal barrier coatings (TBCs), solid oxide fuel cells (SOFCs) and nuclear waste immobilizations. Moreover, the method we developed in this study has a high $Gd_2Zr_2O_7$ nanoparticle yield of up to 89%.

1. Introduction

Gadolinium zirconate ($Gd_2Zr_2O_7$) has two phases, disordered fluorite and ordered pyrochlore. These $Gd_2Zr_2O_7$ phases have promising applications in thermal barrier coatings (TBCs), solid oxide fuel cells (SOFCs) and nuclear waste immobilizations because of low coefficient of thermal conductivity, high ionic conductivity at high temperature, and remarkable resistance to amorphization under ion beam irradiation [1–7]. These physical properties of $Gd_2Zr_2O_7$ have strong dependence on particle size and microstructure. Hence, to ensure their functionality, small size and the preferred microstructure have to be ensured. Compared with coarse-grained ceramics, nanoceramics with crystallite size < 100 nm exhibit enhanced radiation resistance [8], decreased thermal conductivity [9] and superior ionic/electrical conductivity [10,11]. Additionally, the dispersibility and crystallite size of powders also significantly impact the sintering behavior of nanoceramics. Typically, the powders with small particle size and less agglomerate exhibit high sintering activity [12,13]. Therefore, synthesis of $Gd_2Zr_2O_7$ nanoparticles with ultrafine crystallite size and low aggregation is essential and crucial.

Synthesis of $Gd_2Zr_2O_7$ nanoparticles with different pathways have been detailed in earlier reports. Specifically, Ma et al. [14] prepared nearly spherical $Gd_2Zr_2O_7$ particles with different diameters using citric acid combustion (CAC, ~50 nm) and stearic acid combustion (SAC, ~10 nm). Recently, well-crystalized and highly dispersed $Gd_2Zr_2O_7$ nanoparticles with a narrow particle size distribution have been successfully synthesized by Huang et al. [15] using a facile solvothermal method. A homogeneous precipitation-solvothermal method has been reported by Tang et al. for preparation of well-crystallized and dispersed $Gd_2Zr_2O_7$ nanoparticles with grain sizes ranging from 20 to 30 nm [16]. These methods set the foundation for the present study. Moreover, these reports figured out the existing challenges, especially, particle agglomeration [14], large $Gd_2Zr_2O_7$ particle size [16], and complex, multistep synthesis process [15]. Thus, there is a critical need to develop a straightforward, low-cost approach to synthesize monodispersed $Gd_2Zr_2O_7$ nanoparticles with small particle size.

* Corresponding author. College of Physics, Sichuan University, Chengdu, 610064, China.
** Corresponding author. College of Physics, Sichuan University, Chengdu, 610064, China.
E-mail addresses: qijianqi@scu.edu.cn (J. Qi), lutiecheng@scu.edu.cn (T. Lu).

https://doi.org/10.1016/j.ceramint.2019.08.254
Received 13 August 2019; Received in revised form 26 August 2019; Accepted 27 August 2019
Available online 27 August 2019

The LSS (Liquid-solid-solution) phase transfer method, initially reported by Wang et al. [17] in 2005, is based on phase transition and separation during hydrothermal reaction. The LSS phase transfer method have been extensively applied to synthesize small ceramic nanocrystals, including TiO_2, CuO, ZrO_2, SnO_2 and MFe_2O_4 [17–20]. However, to the best of our knowledge, so far, the synthesis of $Gd_2Zr_2O_7$ nanoparticles employing LSS phase transfer method has not been reported. Moreover, there remain two critical issues for the LSS phase transfer method, (1) low yield, and (2) generation of liquid and/or organic chemical wastes, such as spent solvents containing oleic acid and ethyl alcohol.

In this study, we report a modified LSS phase transfer method for the preparation of single-phase $Gd_2Zr_2O_7$ nanoparticles, in which we successfully achieved high yield with minimized generation of chemical waste. Additionally, the mono-dispersed $Gd_2Zr_2O_7$ nanoparticles obtained have a very small average particle size of 1.7 nm. This economical- and environmental-friendly method has promising potential to be used in industrial productions and has great potential to be applied in thermal barrier coatings (TBCs), solid oxide fuel cells (SOFCs) and nuclear waste immobilizations.

2. Experimental methods

The solid starting materials include $Gd(NO_3)_3{\cdot}6H_2O$ (> 99.99%, Ruike RE, China), $Zr(NO_3)_4{\cdot}5H_2O$ (> 99.9%, Chengdu Kelong, China) and sodium oleate (Aladdin). Oleic acid (> 98.0%, Chengdu Kelong, China) and ethyl alcohol were used as solvents. Additionally, ammonium hydroxide aqueous solution (25.0–28.0 %, Chengdu Kelong, China) was added to form surfactant oleylamine to assist the precipitation of Gd^{3+} and Zr^{4+}.

Specifically, 2.178 g of $Gd(NO_3)_3{\cdot}6H_2O$ and 2.071 g of $Zr(NO_3)_4{\cdot}5H_2O$ were dissolved in deionized water (50 ml) in a 200 ml teflon autoclave forming a transparent solution. Subsequently, ethyl alcohol (50 ml), oleic acid (20 ml), sodium oleate (4 g) and ammonium hydroxide (10 ml) were sequentially introduced to the transparent solution, which was transferred to a furnace for hydrothermal reaction at 200 °C for 24 h. The concentrated precipitate at the bottom of teflon autoclave was then collected by outwelling the supernatant liquid. Then, the precipitate was centrifuged and washed by deionized water followed by ethyl alcohol for multiple times to maximize removal of any residual ionic species, such as nitrite and sodium ions. Ultimately, the cleaned product was calcined at elevated temperatures (300, 400, 500, 600 and 700 °C) for 3 h to obtain $Gd_2Zr_2O_7$ nanoparticles.

Fourier transform infrared (FTIR) spectra of the precursor powders were recorded using a TENSOR 27 spectrometer (BRUKER, Germany). The thermogravimetry and differential scanning calorimetry (TG-DSC) analysis of precursor powders was examined using a Netzsch Instrument STA 449 F5 Jupiter system. The TG-DSC experiment was carried out under an air atmosphere from 30 to 1000 °C with a heating rate of 10.0 °C/min. The phase evolutions of the precursor powders were studied using temperature programmed X-ray diffraction (DX-2700, Dandong Fangyuan, Dandong, Liaoning, China) equipped with a *Ni* filtered *Cu Ka* radiation (λ = 1.5406 Å). In the XRD analysis we used a step size of 0.03° in the 2θ range from 10 to 70°. The crystal sizes of all samples were calculated using Scherrer's formula with four crystal planes, (111), (200), (220) and (311). The morphologies of all samples were revealed by transmission electron microscopy (TEM, Tecnai G2 F20 S-TWIN).

3. Results and discussion

The precursor and its calcined products at different temperatures were characterized by FTIR spectra and TG-DSC to reveal the chemical and thermal evolutions during heating, respectively. The FTIR spectra of the precursor and its calcined products at different temperatures are shown in Fig. 1a. The bands at 1452 and 1568 cm^{-1} are attributed to the skeletal vibration of C=C. In addition, the two bands at 2856 and 2925 cm^{-1} are due to the stretching vibration of C–H bond. The observation of C=C and C–H confirms the presence of oleic acid, which enwraps the nanoparticle surface and acting as a surfactant capping ligand [17]. Apparently, as temperature increases, the bands about C–H disappeared completely and the bands about C=C decreases. This demonstrates that oleic acid would be removed at higher temperature and a bit of carbon still exists in the sample. The residual carbon will prevent particle from agglomeration [21]. Absorption bands observed at 3429 to 3431 cm^{-1} are attributed to the stretching vibration of intermolecular hydrogen bonds, which will cause weaker agglomerates [22]. The hydrogen bond forming molecules can be removed during the multiple washing process under centrifuge using ethyl alcohol. Additionally, the characteristic absorption bands at 491 and 493 cm^{-1} are assigned to Zr–O vibrations. The bands observed at 540 cm^{-1} corresponds to Gd–O vibrations, which indicates the formation of metal-oxygen bond below 200 °C.

The TG-DSC and DTG profiles of the precursor are presented in Fig. 1b. Heating in air results in a total mass loss of ~65%. Stepwise weight loss is observed. Specifically, from room temperature to ~350 °C, the sample weight loses 25% due to dehydration and desorption of small organics, resulting in a broad endothermic heat effect. Subsequently, from 350 to 458 °C, larger organics, primarily residual sodium oleate and oleylamine, gradually decompose, followed by gradual weight loss to ~45% and weak endothermic heat effect. After 458 °C further decomposition of residual hydrocarbons in air through combustion is observed, evidenced by the sharp exothermic DSC peak center at 511 °C [23]. The DTG curve suggests the same phenomenon. There appears to be no significant weight loss and exothermic peak at temperature higher than 600 °C. This suggests the completion of organics decomposition and full crystallization of $Gd_2Zr_2O_7$.

The XRD patterns of the precursor and its calcined products at different temperatures are shown in Fig. 2a. The XRD patterns of the precursor powders below 400 °C are in good agreement with the characteristic diffraction peaks of Gd_2O_3 and ZrO_2 mixture. This is consistent with the Zr–O and Gd–O bonds observed in FTIR spectra. As the temperature increases to 400 °C, the XRD peak of Gd_2O_3 disappears, suggesting the formation of $Gd_2Zr_2O_7$ phase at 400 °C. Further temperature increase leads to sharper $Gd_2Zr_2O_7$ XRD. At 700 °C. well crystallized calcined product with a single defect fluorite phase of $Gd_2Zr_2O_7$ (PDF#80-0471) is obtained. In Fig. 2b, the crystallite size calculated by Scherrer's formula is plotted as a function of calcination temperature. Specifically, it is shown that the average grain size of the $Gd_2Zr_2O_7$ nanocrystalline powders calcined at 400 °C is as small as 1.7 nm. Even after calcination at 700 °C, the average crystallite size remains 4.4 nm. The XRD followed by size analysis strongly suggest that our modified LSS method is effective for successful synthesis of single-phase $Gd_2Zr_2O_7$ nanoparticles with ultrafine crystallite size.

After hydrothermal synthesis at 200 °C for 24 h, we dispersed the concentrated precipitate at the bottom of the teflon autoclave in cyclohexane forming a transparent mixture. The TEM image of this transparent mixture is shown in Fig. 3a, which presents monodispersed spherical-shaped nanoparticles with a diameter less than 5 nm. The morphology of $Gd_2Zr_2O_7$ nanoparticles calcined at 700 °C is presented in Fig. 3b, which also shows well-dispersed $Gd_2Zr_2O_7$ nanoparticles without severe aggregation. The average particle size of the calcined $Gd_2Zr_2O_7$ nanoparticles is approximately 5 nm. The dispersity slightly decreases as the calcination temperature increases, which is owing to the coalescing of adjacent particles at higher temperature [24].

Moreover, in our study we also find that the supernatant solution collected after hydrothermal synthesis, containing oleic acid, ethyl alcohol, sodium oleate and oleamide, can be recycled and reused to prepare $Gd_2Zr_2O_7$ nanoparticles of the same quality. The comparison of XRD patterns of $Gd_2Zr_2O_7$ nanoparticles synthesized by initial solvent and recycled supernatant solution is shown in Fig. 4, which exhibits no difference. This highlights that the modified LSS approach is an

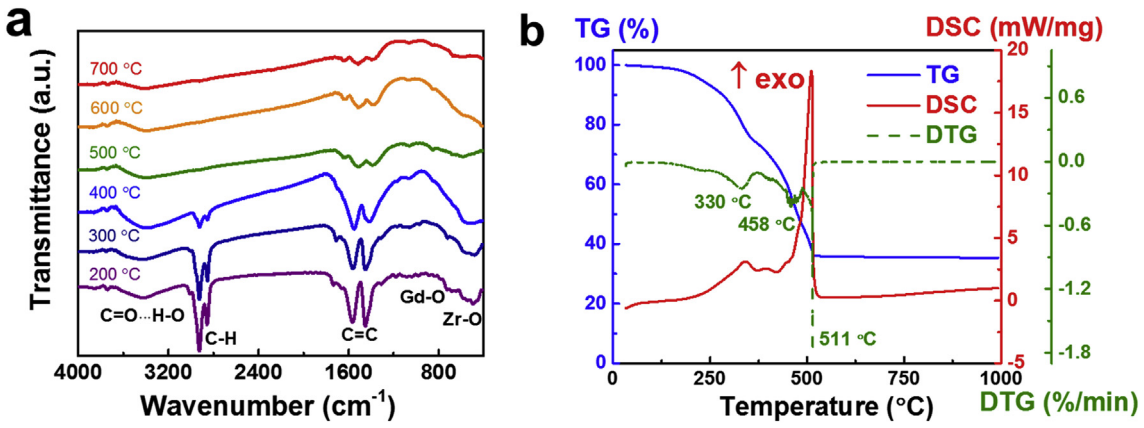

Fig. 1. (a) The FTIR spectra of the precursor after calcination at 200, 300, 400, 500, 600 and 700 °C for 3 h, and (b) the TG-DSC-DTG curve of the precursor calcined in air.

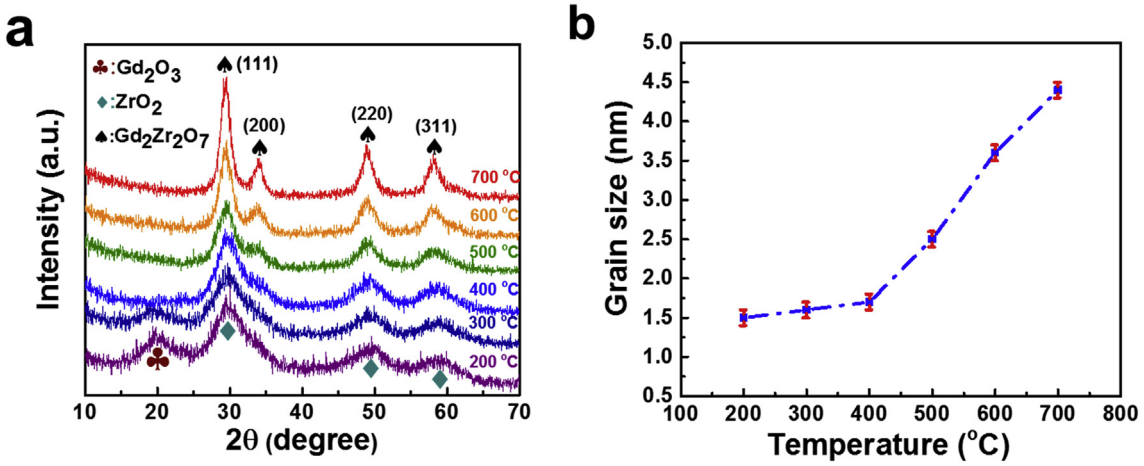

Fig. 2. (a) XRD patterns of the precursor after calcination at 200, 300, 400, 500, 600 and 700 °C for 3 h, and (b) the grain size calculated by Scherrer's formula as a function of calcination temperature.

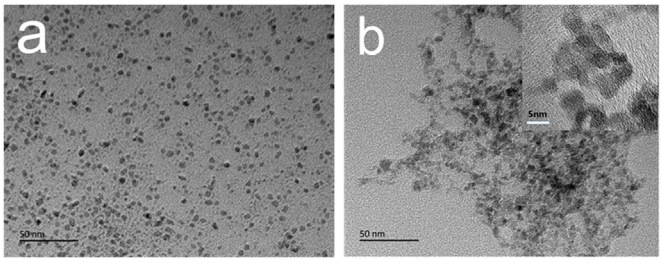

Fig. 3. (a) TEM images of the precursor dissolved in cyclohexane, and (b) $Gd_2Zr_2O_7$ particles obtained from the precursor calcined at 700 °C for 3 h.

economical- and environmental-friendly process, which can be used for production of a large quantity of $Gd_2Zr_2O_7$ materials. Furthermore, very impressively, compared with previously reported yield of 75.4% [25], we increases the yield of $Gd_2Zr_2O_7$ synthesis to 89 %, just as shown in Table 1.

4. Conclusions

In this work, we synthesized monodispersed $Gd_2Zr_2O_7$ nanoparticles using a modified LSS phase transfer method, in which oleic acid and oleamide were employed as capping ligands to control the size of $Gd_2Zr_2O_7$ nanoparticles. According to the XRD results, the average particle size of $Gd_2Zr_2O_7$ is as small as 1.7 nm. This modified LSS phase transfer method enables a straightforward and eco-friendly approach

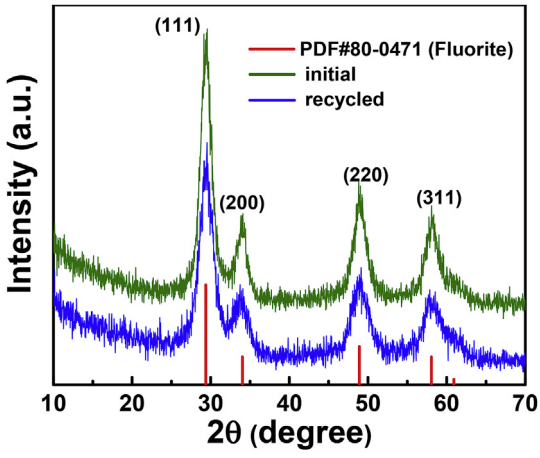

Fig. 4. The XRD patterns of $Gd_2Zr_2O_7$ nanoparticles synthesized from initial solvent (green) and recycled supernatant solution (blue). (For interpretation of the references to colour in this figure legend, the reader is referred to the Web version of this article.)

Table 1
The productive rate of production.

	$Gd(NO_3)_3{\cdot}6H_2O$	$Zr(NO_3)_4{\cdot}5H_2O$	$Gd_2Zr_2O_7$
quality(g)	2.178	2.071	1.298
amount of substance(mol)	0.0048	0.0048	0.0021
productive rate	0.0021/0.0024 = 89%		

for mass-production of nanosized oxide materials with high yield and minimized chemical wastes.

Acknowledgement

This work was supported by the National Natural Science Foundation of China under Grant No. 11775152, the Science and Technology Innovation Team of Sichuan province under Grant NO.15CXTD0025, and the Key Applied Basic Research of Sichuan province under Grant NO. 2017JY0329. Di Wu acknowledges the institutional funds from the Alexandra Navrotsky Institute for Experimental Thermodynamics and Gene and Linda Voiland School of Chemical Engineering and Bioengineering at Washington State University.

References

[1] J. ADıaz-Guillen, M.R. Dıaz-Guillen, JMAlmanza, A.F. Fuentes, J. Santamarıa, C. Leon, Effect of La substitution for Gd in the ionic conductivity and oxygen dynamics of fluorite-type $Gd_2Zr_2O_7$, J. Phys. Condens. Matter 19 (2007) 356212.
[2] M. Li, L. Guo, F. Ye, Phase structure and thermal conductivities of Er_2O_3 stabilized ZrO_2 toughened $Gd_2Zr_2O_7$ ceramics for thermal barrier coatings, Ceram. Int. 42 (2016) 16584–16588.
[3] Z. Huang, N. Ma, J. Qi, X. Guo, M. Yang, Z. Tang, Y. Zhang, Y. Han, D. Wu, T. Lu, Defect-fluorite $Gd_2Zr_2O_7$ ceramics under helium irradiation: amorphization, cell volume expansion, and multi-stage bubble formation, J. Am. Ceram. Soc. 102 (2019) 4911–4918.
[4] X. Lu, X. Shu, X. Liu, Y. Xie, L. Wang, D. Shao, Effects of heavy-ion irradiation on $Gd_2Zr_2O_7$ bearing simulated TRPO waste, Ceram. Int. 44 (2018) 14020–14025.
[5] L. Wang, J.I. Eldridge, S.M. Guo, Thermal radiation properties of plasma-sprayed $Gd_2Zr_2O_7$ thermal barrier coatings, Scr. Mater. 69 (2013) 674–677.
[6] L. Peng, K. Zhang, Z. He, D. Yin, J. Xue, C. Xu, H. Zhang, Self-propagating high-temperature synthesis of ZrO_2 incorporated $Gd_2Ti_2O_7$ pyrochlore, J. Adv. Ceram. 7 (2017) 41–49.
[7] Z. Wang, G. Zhou, D. Jiang, S. Wang, Recent development of $A_2B_2O_7$ system transparent ceramics, J. Adv. Ceram. 7 (2018) 289–306.
[8] J. Zhang, J. Lian, A.F. Fuentes, F. Zhang, M. Lang, F. Lu, R.C. Ewing, Enhanced radiation resistance of nanocrystalline pyrochlore $Gd_2(Ti_{0.65}Zr_{0.35})_2O_7$, Appl. Phys. Lett. 94 (2009) 243110.
[9] G. Soyez, J.A. Eastman, L.J. Thompson, G.R. Bai, P.M. Baldo, A.W. McCormick, R.J. DiMelfi, A.A. Elmustafa, M.F. Tambwe, D.S. Stone, Grain-size-dependent thermal conductivity of nanocrystalline yttria-stabilized zirconia films grown by metal-organic chemical vapor deposition, Appl. Phys. Lett. 77 (2000) 1155–1157.
[10] Y.W. Zhang, S. Jin, Y. Yang, G.B. Li, S.J. Tian, J.T. Jia, C.S. Liao, C.H. Yan, Electrical conductivity enhancement in nanocrystalline $(RE_2O_3)_{0.08}(ZrO_2)_{0.92}$ (RE = Sc, Y) thin films, Appl. Phys. Lett. 77 (2000) 3409–3411.
[11] M.G. Bellino, D.G. Lamas, N.E.W.d. Reca, Enhanced ionic conductivity in nanostructured, heavily doped ceria ceramics, Adv. Funct. Mater. 16 (2006) 107–113.
[12] H. Ferkel, R.J. Hellmig, Effect of nanopowder deagglomeration on the densities of nanocrystalline ceramic green bodies and their sintering behaviour, Nanostructured Mater. (1999) 11.
[13] J. Wang, F. Long, W. Wang, S. Mo, Z. Zou, Z. Fu, Reaction coupling preparation of high sintering activity boron carbide nano-powders, Ceram. Int. 42 (2016) 6969–6977.
[14] L. Ma, W. Ma, X. Sun, J. Liu, L. Ji, H. Song, Structure properties and sintering densification of $Gd_2Zr_2O_7$ nanoparticles prepared via different acid combustion methods, J. Rare Earths 33 (2015) 195–201.
[15] Z. Huang, J. Qi, M. Zhou, Y. Gong, Q. Shi, M. Yang, W. Han, Z. Cao, S. Peng, T. Lu, A facile solvothermal method for high-quality $Gd_2Zr_2O_7$ nanopowder preparation, Ceram. Int. 44 (2018) 1334–1342.
[16] Z. Tang, Z. Huang, J. Qi, X. Guo, W. Han, M. Zhou, S. Peng, T. Lu, Synthesis and characterization of $Gd_2Zr_2O_7$ defect-fluorite oxide nanoparticles via a homogeneous precipitation-solvothermal method, RSC Adv. 7 (2017) 54980–54985.
[17] X. Wang, J. Zhuang, Q. Peng, Y. Li, A general strategy for nanocrystal synthesis, Nature 437 (2005) 121–124.
[18] F. Huang, D. Chen, J. Zhou, Y. Wang, Modifying the phase and controlling the size of monodisperse ZrO_2 nanocrystals by employing Gd^{3+} as a nucleation agent, CrystEngComm 13 (2011) 4500.
[19] X. Yang, F. Huang, Z. Huang, F. Cao, J. Zhang, Small-size and monodispersed red-emitting Pr^{3+} doped barium molybdate nanocrystals with ultrahigh color purity, RSC Adv. 6 (2016) 65311–65314.
[20] Y. Zhu, X. Lv, L. Zhang, X. Guo, D. Liu, J. Chen, J. Ji, Liquid-solid-solution assembly of $CoFe_2O_4$/graphene nanocomposite as a high-performance lithium-ion battery anode, Electrochim. Acta 215 (2016) 247–252.
[21] Z. Quan, D. Wu, J. Zhu, W.H. Evers, J.M. Boncella, L.D.A. Siebbeles, Z. Wang, A. Navrotsky, H. Xu, Energy landscape of self-assembled superlattices of PbSe nanocrystals, Proc. Natl. Acad. Sci. 111 (2014) 9054–9057.
[22] A. Gemma, E. Mayans, G. Ballano, J. Torras, A. Díaz, A.I. Jiménez, J. Puiggalí, C. Cativiela, C. Alemán, Self-assembly of diphenylalanine with preclick components as capping groups, Phys. Chem. Chem. Phys. 19 (2017) 27038–27051.
[23] M.G. Mothé, C.G. Mothé, C.H.M. Carvalho, M.C.K.d. Oliveira, Thermal evaluation of heavy crude oil by simultaneous TG-DSC-FTIR: Part 2, J. Therm. Anal. Calorim. 117 (2014) 1357–1363.
[24] W. Lu, H. Schmidt, Synthesis of nanosized $BaSnO_3$ powders from metal isopropoxides, J. Sol. Gel Sci. Technol. 42 (2006) 55–64.
[25] Y. Li, K. Ji, X. Liu, X. Zhao, Y. Gao, W. Deng, Y. Liu, Preparation of nano-silver powders by hydrothermal liquid-solid-solution method and characterization, Precious Met. 38 (No.2) (2017).